Electronic Supplementary Material (ESI) for Environmental Science: Nano.
This journal is © The Royal Society of Chemistry 2022

An insight into the bridging role of Co_3O_4 in MOF-derived binary metal oxides modified sheet-like g-C_3N_4 for photo-assisted peroxymonosulfate activation

Guangfu Wang [a,b], Danlian Huang [a,b,*], Min Cheng [a,b,*], Sha Chen [a,b], Gaoxia Zhang [c], Li Du [a,b], Lei Lei [a,b], Yashi Chen [a,b], Ruijin Li [a,b], Yang Liu [a,b]

[a.] *College of Environmental Science and Engineering, Hunan University, Changsha, Hunan 410082, China*

[b.] *Key Laboratory of Environmental Biology and Pollution Control (Hunan University), Ministry of Education, Changsha, Hunan 410082, China*

[c.] *Carbon Neutrality Research Institute of Power China Jiangxi Electric Power Construction Co., Ltd., Nanchang 330001, China*

---

* Corresponding author at: College of Environmental Science and Engineering, Hunan University, Changsha, Hunan 410082, China.

Tel.: +86-731- 88822754; fax: +86-731-88823701.

E-mail address: huangdanlian@hnu.edu.cn (D.L. Huang), chengmin@hnu.edu.cn (M. Cheng).

2. Materials and methods

2.2 Catalyst characterization and photoelectrochemical measurements

The results of crystal structure in as-prepared catalysts were obtained by powder X-ray diffraction (XRD, Bruker D8 advance) with Cu-Kα irradiation. Chemical groups and bonds were tested by Fourier transform infrared (FTIR). Scanning electron microscope (SEM, FEI Verios 460) was performed to observe the morphology topography of samples, while Transmission electron microscope (TEM, TecnaiG2 F20 S-TWIN TMP) was used to analyze their interior structure and crystal lattice properties. Brunauer-Emmett-Teller (BET, Micromeritics ASAP 2460 3.01) was employed to evaluate the specific surface area (S_{BET}), pore volume as well as pore size distribution. The element composition and state were obtained by the investigation of X-ray photoelectron spectroscopy (XPS, Thermo Scientific K-Alpha+) test.

The absorption of light in the range of 200-800 nm by the material was known from ultraviolet-visible diffuse reflectance spectroscopy (DRS, Cary 300 UV-vis) tests. The compounding efficiency of photogenerated carriers was reflected by the Photoluminescence (PL, PerkinElmer LS-55 fluorescence spectrophotometer) spectra, in which samples were excited by 320 nm fluorescence. The electrochemical station (CHI 760E) was employed to figure out the photocurrents and electrochemical impedance spectroscopy (EIS) state. The construction of a three-electrode system included working electrode (samples with 1 cm^2 active area on FTO glass), counter electrode (platinum) and reference electrode (saturated calomel electrode) with 0.2 M

Na_2SO_4 solution as the electrolyte. For photocurrent test, 300 W Xe lamp with 420 nm cutoff filter provided the periodic visible light irradiation to the working electrode for generation of chopped-light amperometric I-t characterizations. EIS was measured within the frequency ranging from 10^5 to 10^{-2} Hz in an AC voltage amplitude of 0.18 V. The electron spin resonance (ESR) signal of radicals was reflected with 5,5-dimethyl-1-pyrroline N-oxide (DMPO), 2,2,6,6-Tetramethylpiperidine (TEMP) and TEMPO as spin-trapping agents.

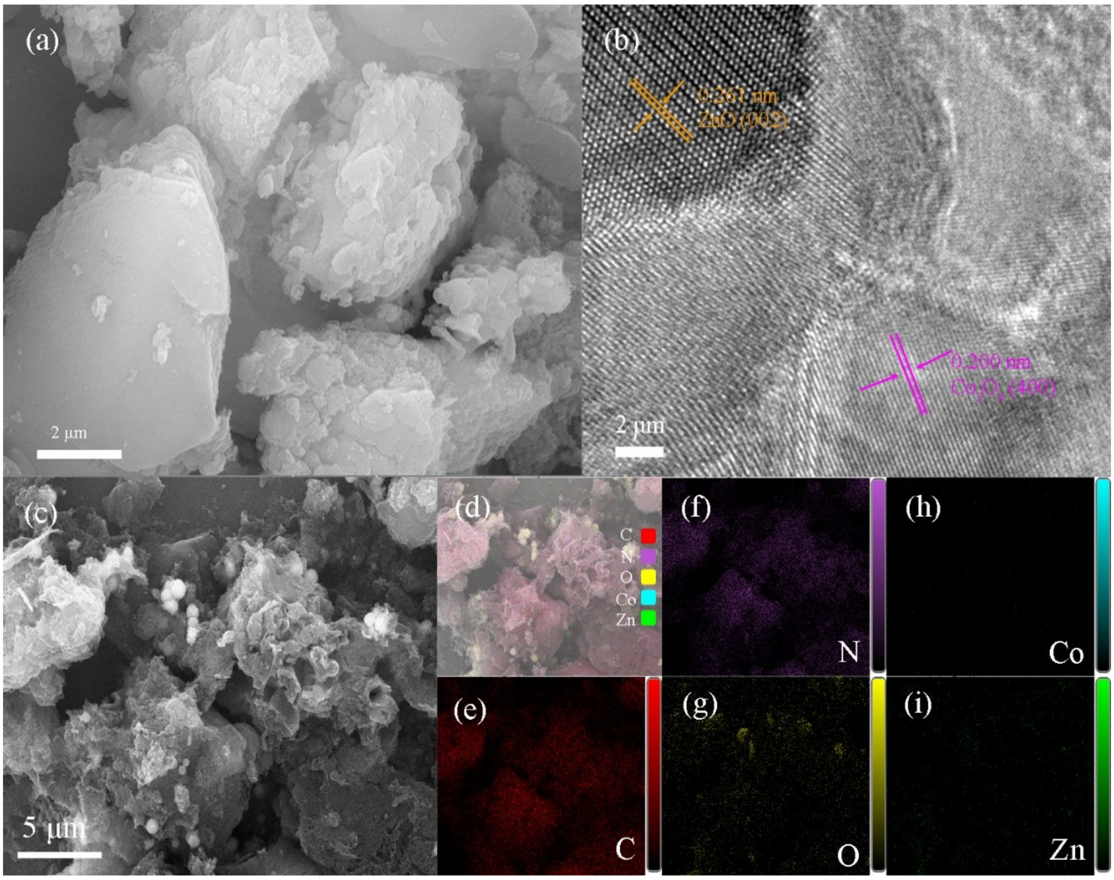

Fig. S1 SEM image of BCN (a); HRTEM of ZCC-SCN$_{10}$ (d); EDX mapping of each element (c-i).

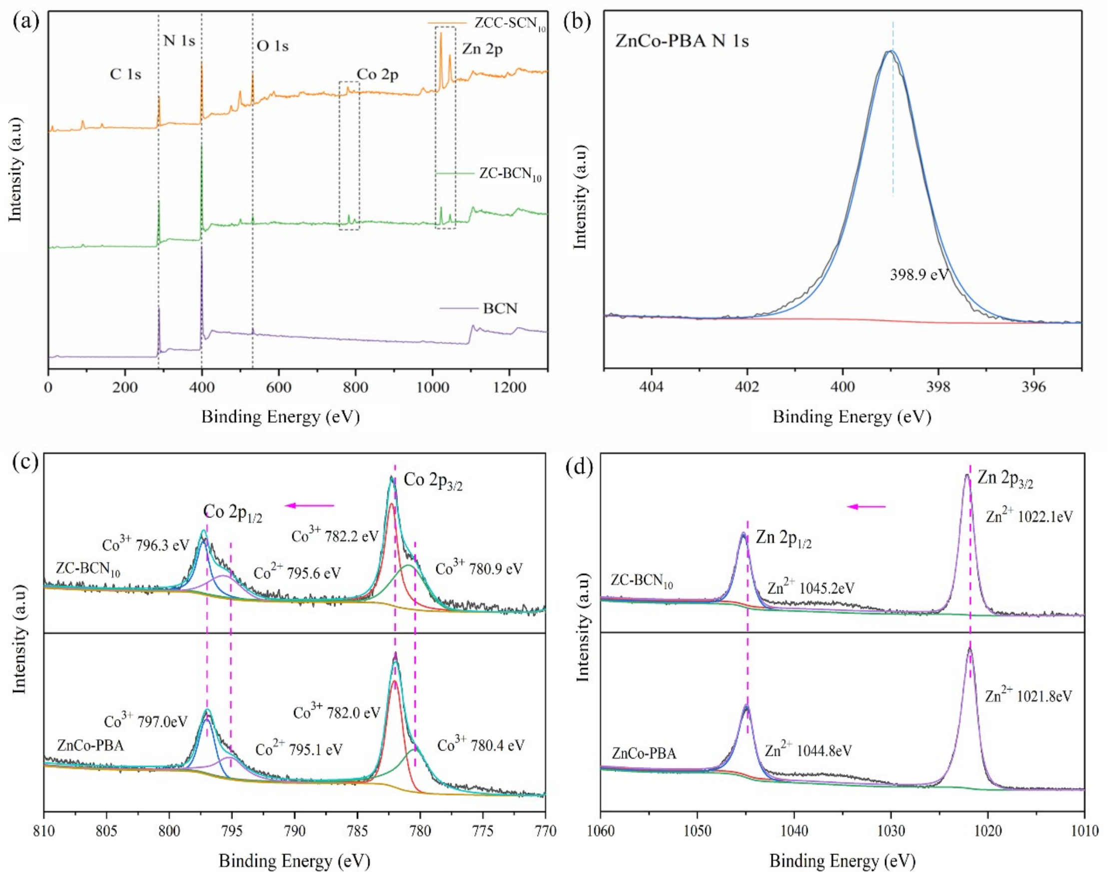

Fig. S2 Wide-range XPS spectra of samples (a) and N 1s spectrum of ZnCo-PBA (b). Co 2p spectra (c); Zn 2p spectra (d) of ZnCo-PBA and ZC-BCN$_{10}$.

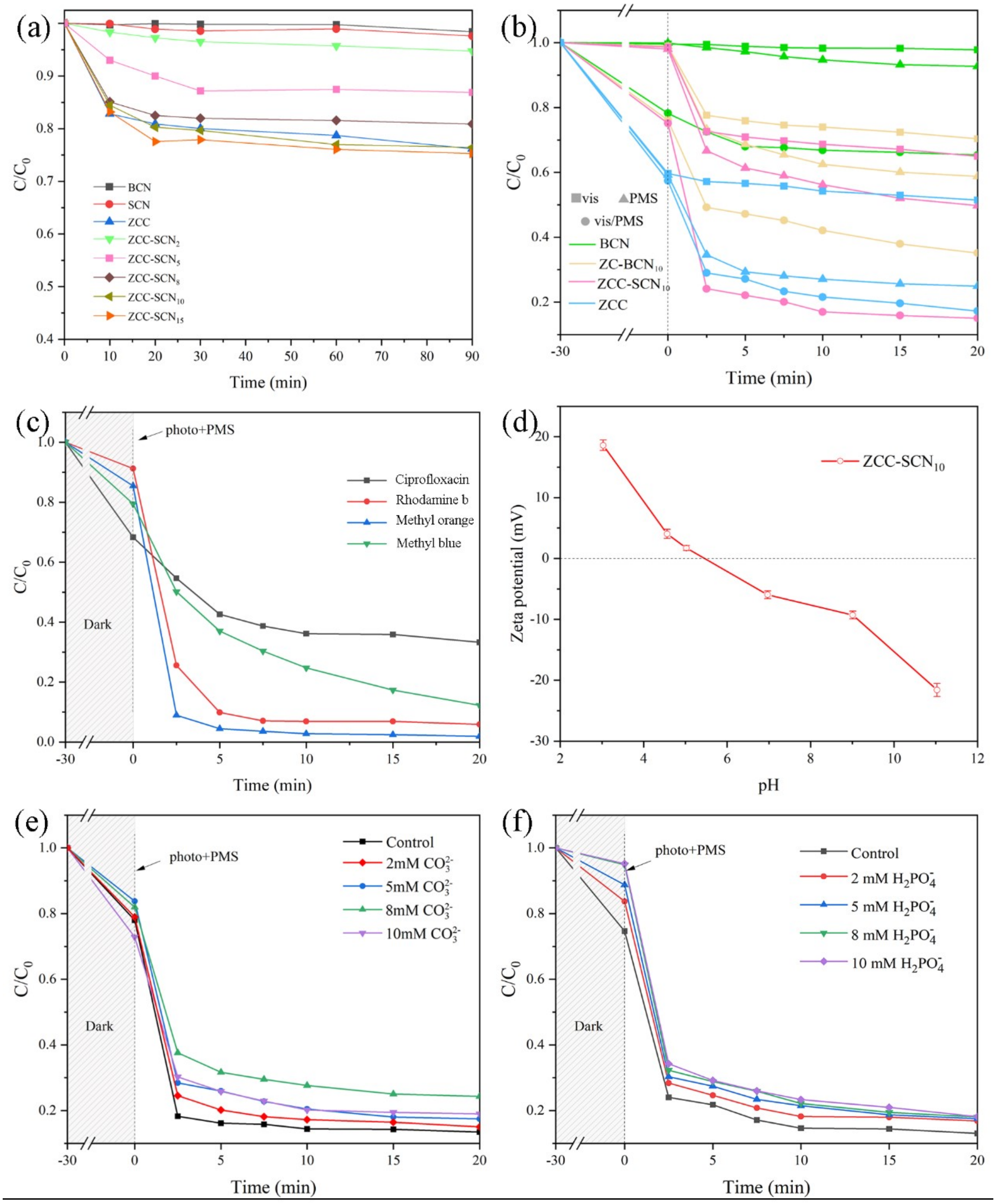

Fig. S3 (a) Adsorption equilibrium curve of the sample on TC-HCl; (b) photocatalytic activities and PMS activation capacities of TC-HCl degradation over samples; (c) catalytic degradation for different pollutants by ZCC-SCN$_{10}$; (d) zeta potential of the ZCC-SCN$_{10}$ at different pH; effect of (e) HCO_3^-, (f) $H_2PO_4^-$ on TC-HCl degradation with ZCC-SCN$_{10}$. ([catalyst]$_0$=0.2 g/L; [pollutant]$_0$=20 mg/L).

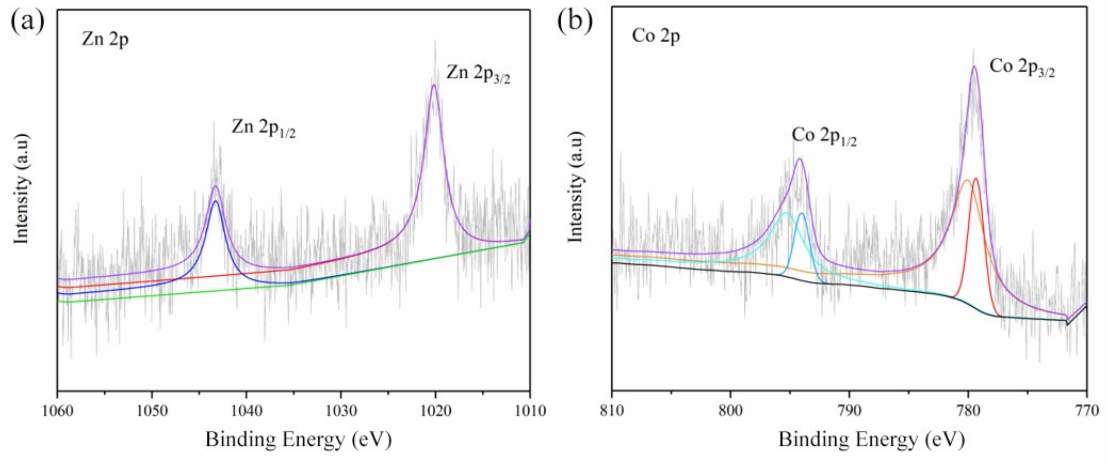

Fig. S4 High-resolution Zn 2p (a) and Co 2p (b) XPS spectra of ZCC-SCN_{10}.

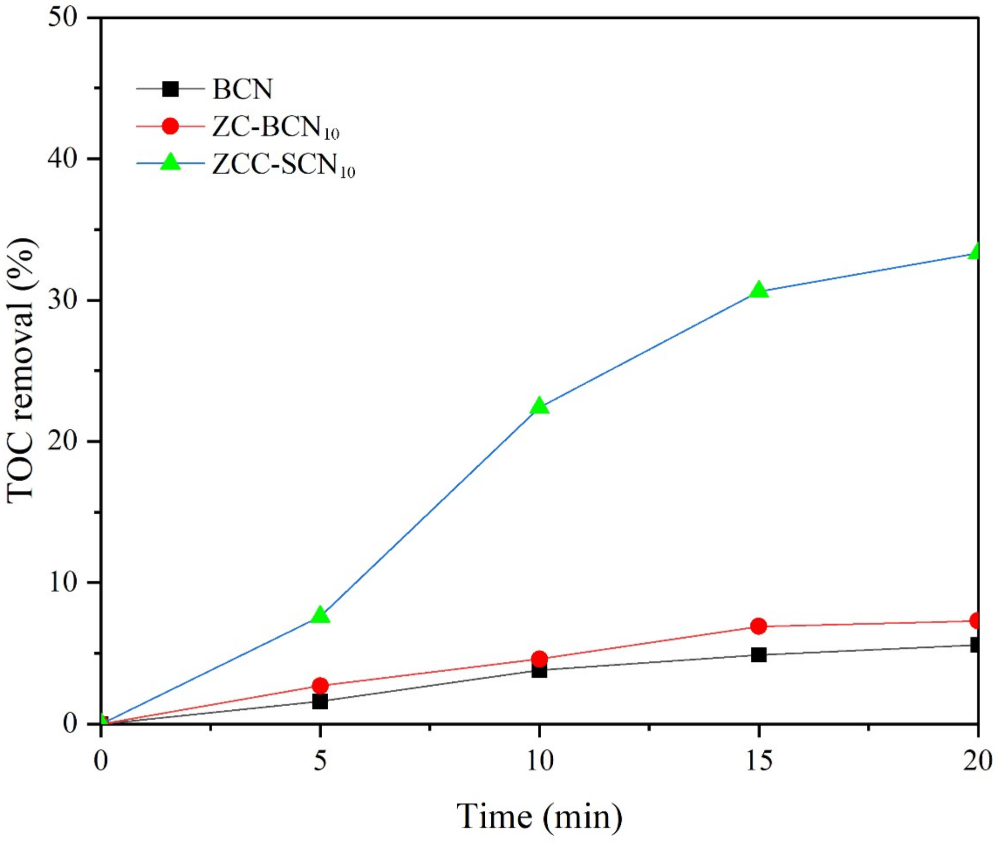

Fig. S5 TOC removal efficiency of BCN, ZC-BCN_{10} and ZCC-SCN_{10}.

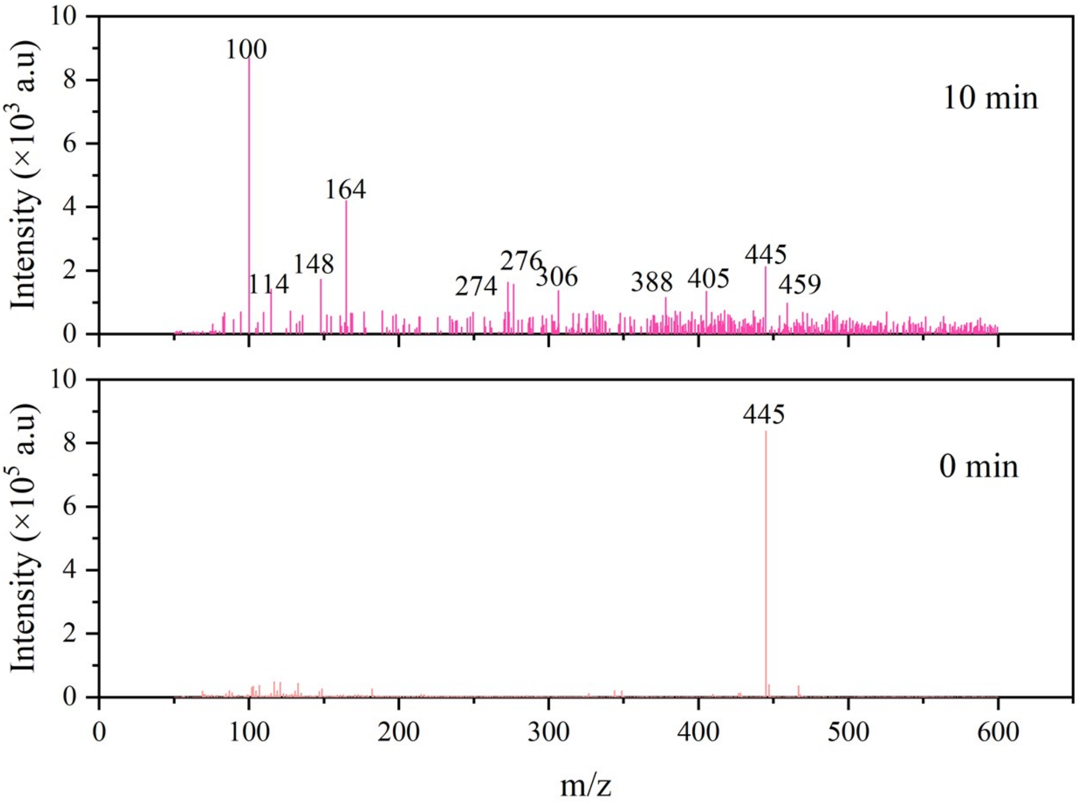

Fig. S6 HPLC-MS test for TC-HCl degradation in 0 min and 10 min of ZCC-SCN$_{10}$/vis/PMS system.

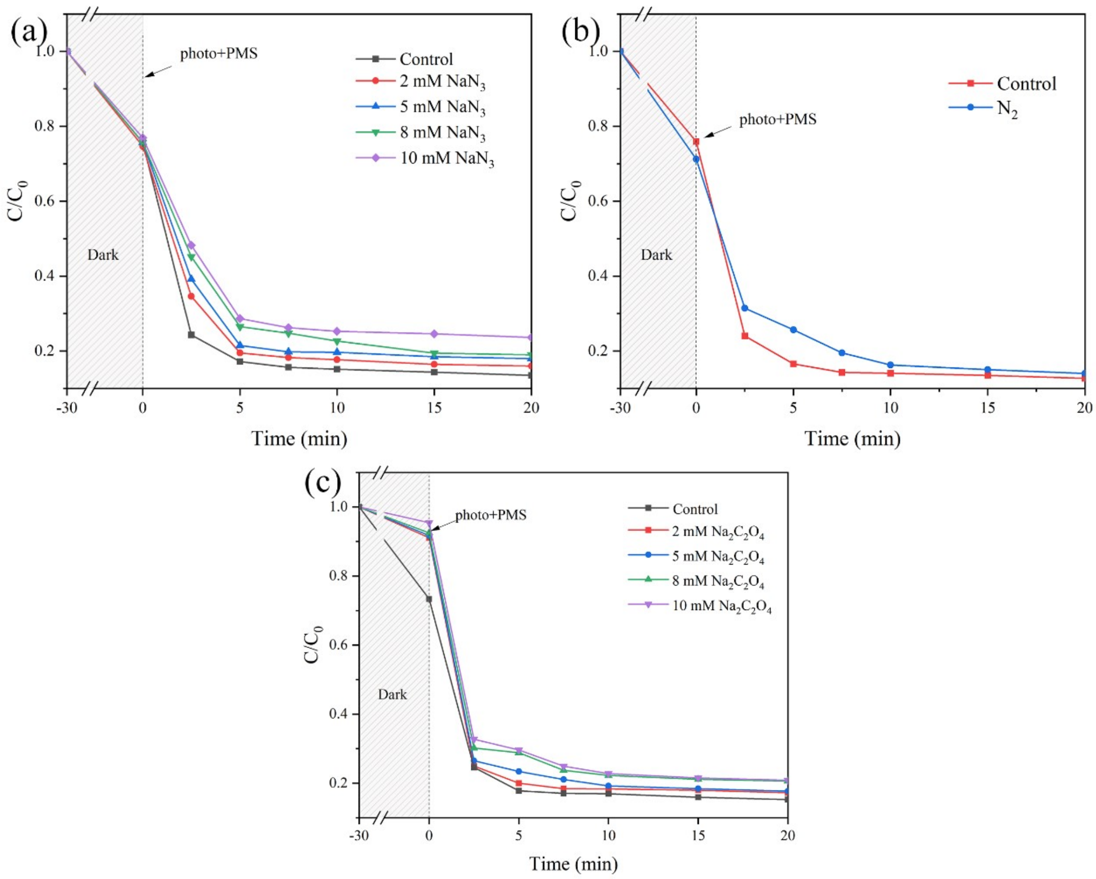

Fig. S7 Effects of (a) NaN_3 quenching, (c) $Na_2C_2O_4$ quenching on HTC degradation. ($[catalyst]_0$=0.2 g/L; $[PMS]_0$=0.15 g/L; $[HTC]_0$=20 mg/L).

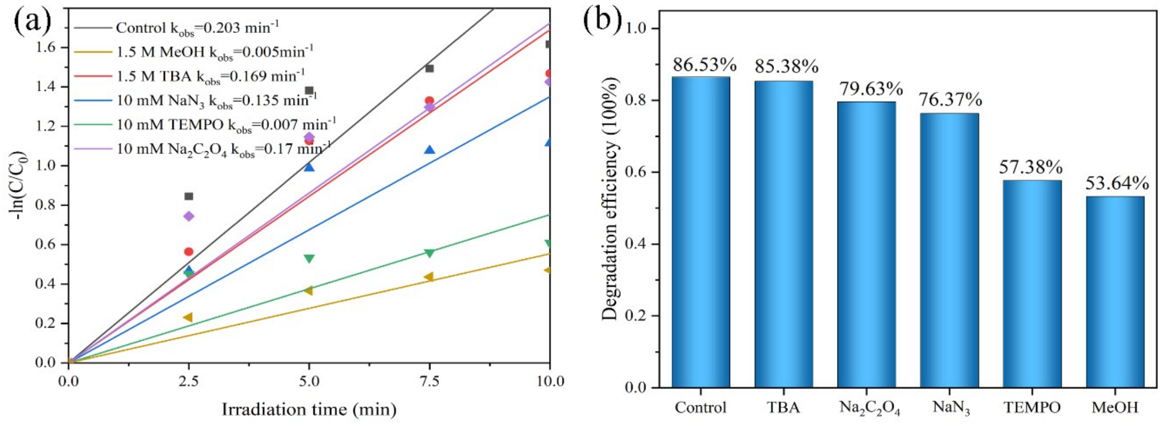

Fig. S8(a) The calculated corresponding k_{obs} of free radical capture groups; (b) Degradation efficiency of free radical capture experiments.

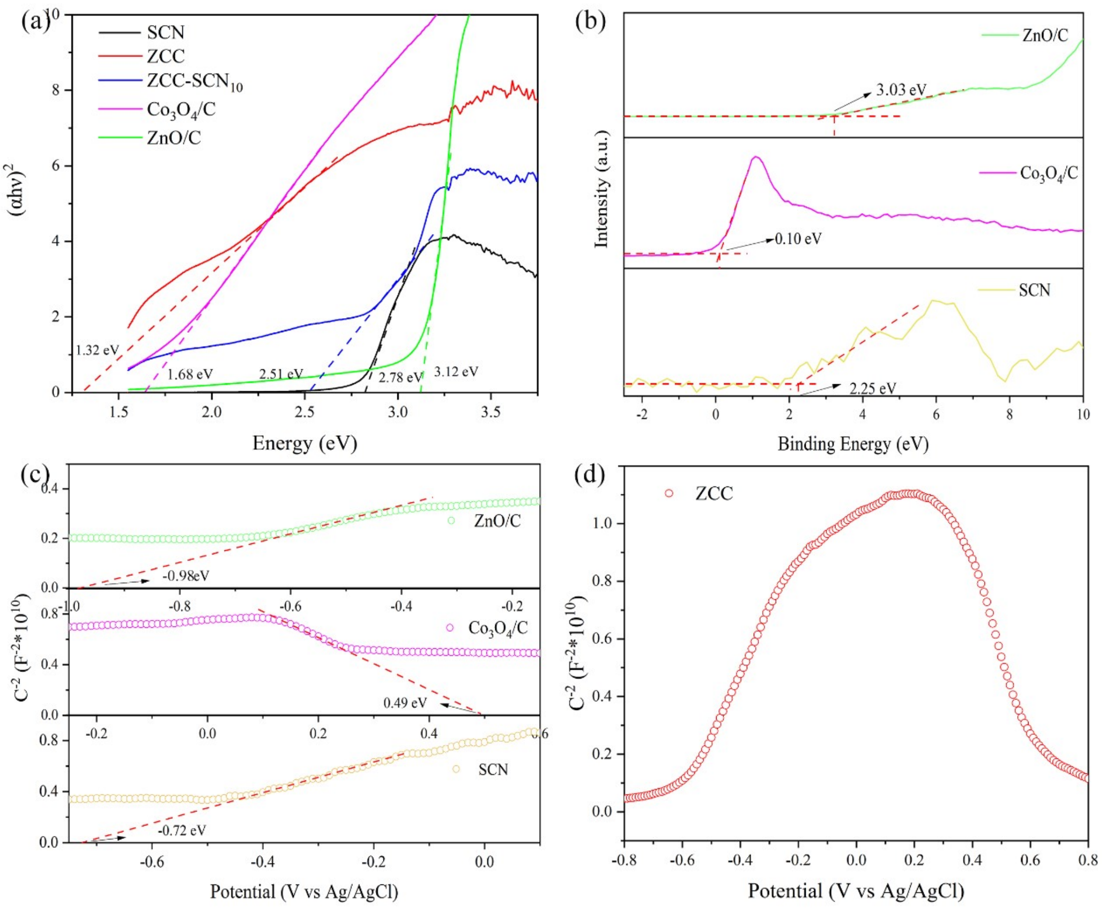

Fig. S9 Tauc relation plots of samples (a); VB-XPS spectra of SCN, Co_3O_4 and ZnO (b); Mott-Schottky plots of SCN, Co_3O_4 and ZnO (c) and ZCC (d).

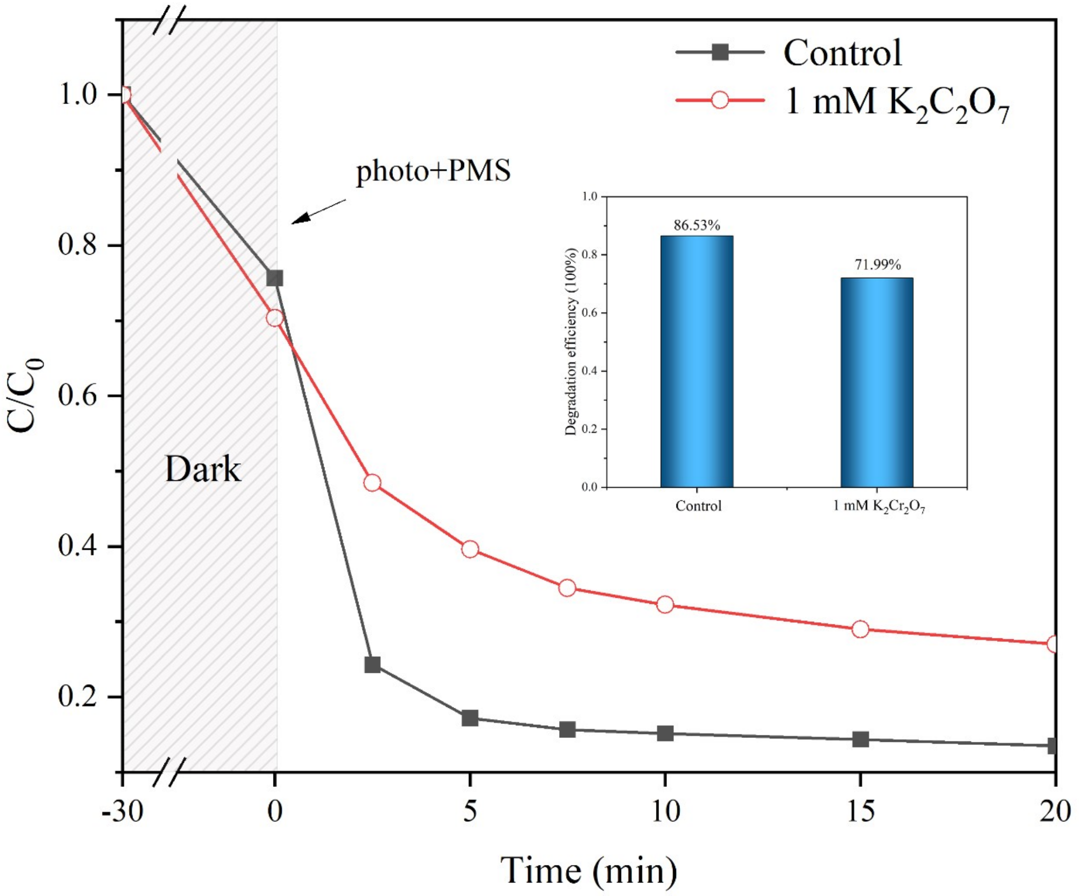

Fig. S10 Effect of $K_2Cr_2O_7$ (electronic suppression) on TC-HCl degradation with ZCC-SCN_{10}. ($[catalyst]_0$=0.2 g/L; $[PMS]_0$=0.2 g/L; $[TC\text{-}HCl]_0$=20 mg/L).

Table S1 The specific surface area and pore distribution of the samples.

Samples	S_{micro} (m^2/g) S_{BET} (m^2/g)	S_{micro}/S_{BET}(%)	V_{pore} (m^3/g) V_{micro} (m^3/g)	V_{micro}/V_{pore} (%)
BCN	2.55 12.50	20.41	0.001 0.081	1.47
ZC-BCN	34.85 56.13	62.09	0.014 0.093	15.48
ZCC-SCN	9.75 81.84	11.92	0.004 0.394	1.02

Table S2 Atomic changes of Co^{II} and Co^{III} in ZCC-SCN_{10}.

	Original ZCC-SCN_{10}		Used ZCC-SCN_{10}		Used ZCC-SCN_{10} (electron suppression)	
	Binding Energy (eV)	Atomic %	Binding Energy (eV)	Atomic %	Binding Energy (eV)	Atomic %
Co^{II}	780.0/795.4	62.92	780.1/795.3	74.15	780.6/796.3	51.09
Co^{III}	778.5/793.5	27.46	779.3/794.0	18.92	779.5/794.5	36.32
Co sat.	787.6/802.8	8.62	784.5/803.1	6.70	788.5/804.1	12.29